RSC Advances

PAPER

Cite this: *RSC Adv.*, 2025, **15**, 17503

Synthesis of 4*H*-pyrimido[2,1-*b*]benzimidazoles catalyzed by a Schiff base cobalt(II) complex supported on cobalt ferrite magnetite nanoparticles†

Ahmad Reza Moosavi-Zare, *[ba] Zahra Darvishi,[a] Hamid Goudarziafshar[a] and Abedien Zabardasti[c]

Received 25th April 2025
Accepted 26th April 2025

DOI: 10.1039/d5ra02906f

rsc.li/rsc-advances

Nano-[$CoFe_2O_4$@SiO_2/propyl-1-(*o*-vanillinaldimine)][$CoCl_2$] was designed and reported with the Schiff base cobalt(II) complex anchored onto cobalt ferrite magnetite nanoparticles. The resulting nanomagnetite Schiff base cobalt(II) complex was employed as a recoverable catalyst for the condensation reaction of aryl aldehyde, 2-aminobenzimidazole and ethyl acetoacetate at 90 °C to synthesize 4*H*-pyrimido[2,1-*b*]benzimidazoles under solvent-free condition. According to the proposed mechanism, the cobalt complex can accelerate the reaction *via* a structural rearrangement from a tetrahedral to a square planar geometry.

1. Introduction

4*H*-Pyrimido[2,1-*b*]benzimidazoles are important heterocycles that have attracted the attention of chemists due to their significant medicinal properties. Antitumor,[1] anti-inflammatory,[2] antifungal[3] and antibacterial activities[4] are among the notable biological properties observed in this class of compounds.

The multicomponent synthesis of 4*H*-pyrimido[2,1-*b*]benzimidazoles through the condensation of a β-keto ester with 2-aminobenzimidazole and various aldehydes is one of the most common protocols for preparing this class of compounds.[5] Multicomponent condensation reactions are significant in green chemistry, as they allow the synthesis of the desired product in a single step without the need to isolate reaction intermediates. Savings in raw materials and solvents, compliance with atom economy and reduced waste generation are important advantages of this protocol. Additional benefits include reduced reaction time, increased product yield, fewer synthesis steps and a shortened purification process.[6–17]

The synthesis of 4*H*-pyrimido[2,1-*b*]benzimidazoles has previously been reported *via* a one-pot, three-component condensation reaction of various aryl aldehydes with a β-keto ester and 2-aminobenzimidazole, using different catalysts such as H_3PO_4–Al_2O_3,[18] TMGT,[19] $TiCl_2$/cellulose,[20] GO@PSA-Cu,[21] nano-acetic acid,[22] [bmim]BF_4,[23] 1,3-disulfonic acid imidazolium trifluoroacetate,[24] poly(vinylpyrrolidonium) perchlorate,[25] thiamine hydrochloride (VB_1),[26] TiO_2/porous carbon,[27] poly(*N*-bromo-*N*-ethylbenzene-1,3-disulfonamide),[28] nano-[Co–4CSP]Cl_2,[29] [NSPy]$ZnCl_3$,[30] Na^+–MMT–[pmim]HSO_4,[31] Na^+-montmorillonite perchloric acid,[32] Fe_3O_4@SiO_2@L-glutamine NPs[33] and sodium acetate.[34] Considering the medicinal importance of these compounds, it is important to introduce new protocols and design efficient catalysts for their synthesis.

In the present work, a nanomagnetic heterogeneous catalyst was designed and introduced for the preparation of 4*H*-pyrimido[2,1-*b*]benzimidazoles. Reducing the catalyst size to the nanoscale induced significant qualitative changes in its structure and catalytic performance.[35,36] Producing a catalyst at the nanoscale increased its contact surface with the reactants, thereby enhancing the reaction efficiency. One of the most important advantages of heterogeneous catalysts is their ease of separation from the reaction medium.[37–40]

The use of magnetic nanoparticles in chemical reactions, and the design of catalysts of this size with magnetic properties, such as core–shell and supported catalysts, have received much attention. Designing catalysts with magnetic components facilitates easier recovery and reuse, resulting in significant savings in chemical consumption. In addition to their catalytic ability, magnetic nanoparticles have been widely used in other applications such as drug delivery and removal of inorganic and organic pollutants from the environment.[41–45]

Building on the above facts and the continued use of Schiff base complexes as catalysts in organic synthesis,[46–48] a novel Schiff

[a]*Department of Chemical Engineering, Hamedan University of Technology, Hamedan, 65155, Iran. E-mail: moosavizare@yahoo.com*

[b]*Chemistry Department, College of Sciences, Shiraz University, Shiraz 71946-84795, Iran*

[c]*Department of Inorganic Chemistry, Faculty of Chemistry, Lorestan University, Khorramabad 68151-44316, Iran*

† Electronic supplementary information (ESI) available. See DOI: https://doi.org/10.1039/d5ra02906f

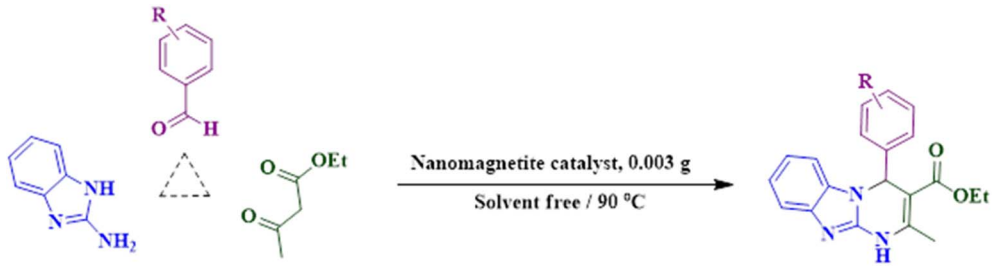

Scheme 1 Preparation of 4*H*-pyrimido[2,1-*b*]benzimidazoles using a nanomagnetite catalyst.

base cobalt(II) complex was designed and immobilized on cobalt ferrite magnetite nanoparticles to be used as a recoverable catalyst for the three-component synthesis of 4*H*-pyrimido[2,1-*b*]benzimidazoles at 90 °C under solvent-free conditions (Scheme 1).

2. Experimental section

All materials were purchased from Merck and used without further purification, and their purity was checked by thin-layer chromatography (TLC). The melting point of the products were measured using an Electrothermal 9100 instrument. Nuclear magnetic resonance (^{1}H NMR and ^{13}C NMR) spectra were recorded on a Bruker DRX-250 Avance spectrometer with deuterated DMSO as a solvent. Infrared spectra of the products were recorded on a PerkinElmer PE-1600-FTIR instrument.

2.1. Synthesis of nano [$CoFe_2O_4$@SiO_2/propyl-1-(*o*-vanillinaldimine)][$CoCl_2$]

3-Aminopropyltriethoxysilane (1.0 mmol) was added to *ortho*-vanillin (1.0 mmol) in a round bottom flask connected to a reflux condenser at room temperature, in the absence of solvent, and stirred for 24 h to prepare $(OEt)_3$Si/propyl-1-(*o*-vanillinaldimine). To metallise the Schiff base ligand in the previous step, $(OEt)_3$Si/propyl-1-(*o*-vanillinaldimine) (2 mmol) was added to a mixture of $CoCl_2 \cdot 6H_2O$ (1 mmol) and toluene (10 mL) in a round bottom-flask connected to a reflux condenser, and the mixture was stirred under reflux for 24 h to afford the cobalt(II) Schiff base complex. Then, the obtained cobalt(II) complex (1 mmol) was added to a round-bottom flask connected to a reflux condenser containing toluene (20 mL) and $CoFe_2O_4$@SiO_2 nanoparticles (2 g), which were prepared according a previous report,[49] and stirred under reflux for 24 h to prepare the nanomagnetite complex as the main catalyst. Finally, for further purification, the catalyst was washed twice with ethanol and dried in a thermal oven at 60 °C.

2.2. General procedure for the preparation of 4*H*-pyrimido[2,1-*b*]benzimidazole derivatives

An aromatic aldehyde (1 mmol), 2-aminobenzimidazole (1 mmol, 0.133 g), ethyl acetoacetate (1 mmol, 0.13 g) and

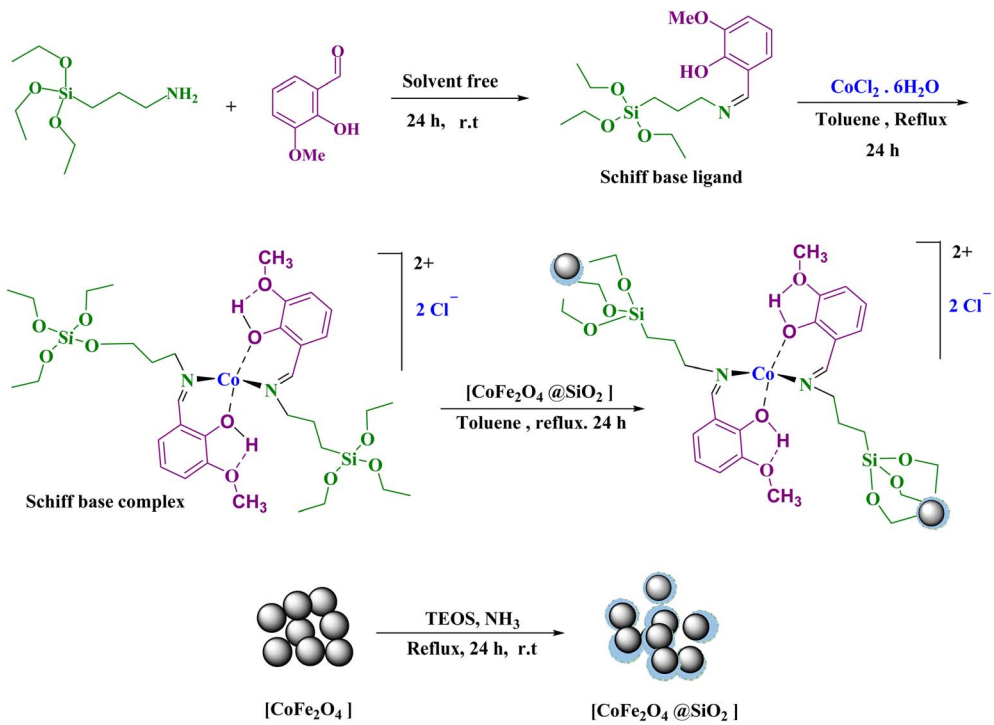

Scheme 2 Preparation of nano-[$CoFe_2O_4$@SiO_2/propyl-1-(*o*-vanillinaldimine)][$CoCl_2$].

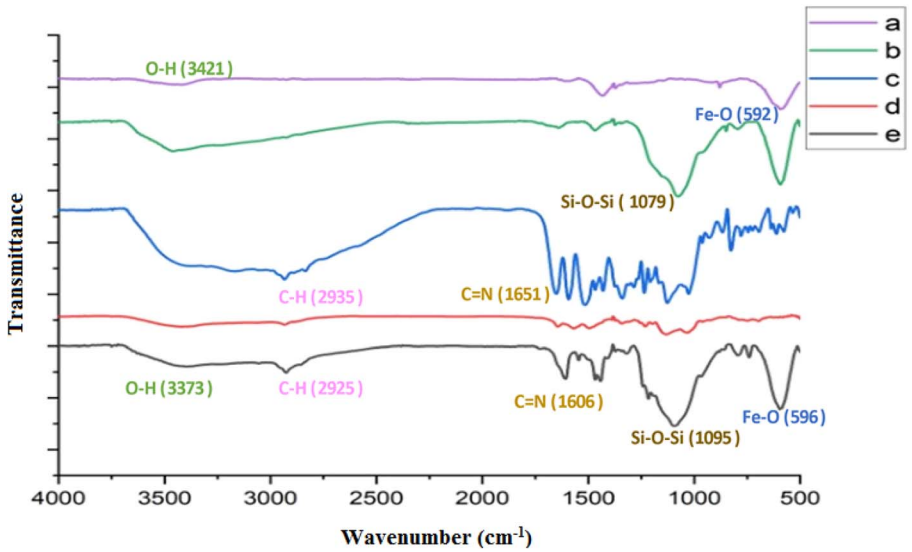

Fig. 1 FT-IR spectrum of nano-[$CoFe_2O_4$@SiO_2/propyl-1-(*o*-vanillinaldimine)][$CoCl_2$] in comparison with other species in the structure of the catalyst: (a) $CoFe_2O_4$, (b) $CoFe_2O_4$@SiO_2, (c) Schiff base ligand, (d) Schiff base complex, (e) main catalyst.

[$CoFe_2O_4$@SiO_2/propyl-1-(*o*-vanillinaldimine)][$CoCl_2$] (3 mg) as a catalyst were added to a 25 mL round-bottomed flask connected to a reflux condenser and stirred at 90 °C in the absence of solvent. After completion of the reaction, as monitored by TLC, warm ethanol (10 mL) was added to extract the product, and the catalyst was separated from the reaction mixture using an external magnet. Lastly, the expected product was purified by recrystallization from ethanol (90%).

2.3. Spectral data of compounds

2.3.1 Compound (2). White solid; IR (KBr), ν: 479, 742, 757, 795, 1085, 1255, 1460, 1520, 1576, 1699, 2925, 3101, 3432 cm^{-1}; ^1H NMR (250 MHz, DMSO-d_6), δ_{ppm}: 1.06 (t, J = 7.50 Hz, 3H, CH_3), 2.45 (s, 3H, CH_3), 3.96 (d, J = 7.5o Hz, 2H, CH_2), 6.73 (s, 1H, CH), 6.94 (d, J = 7.50 Hz, 1H, ArH), 7.01 (d, J = 5.00 Hz, 1H, ArH), 7.16–7.23 (m, 3H, ArH), 7.23–7.31–7.34 (m, 2H, ArH), 7.41 (s, 1H, ArH), 10.89 (s, 1H, NH); ^{13}C NMR (62.5 MHz, DMSO-d_6):

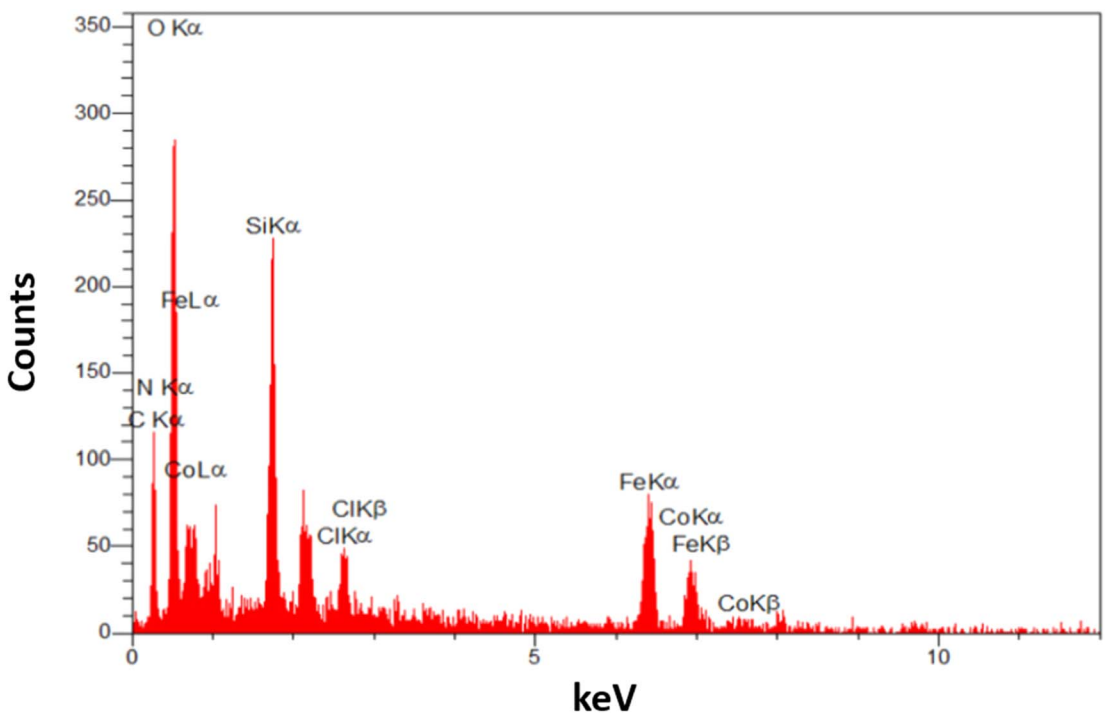

Fig. 2 EDX analysis of nano-[$CoFe_2O_4$@SiO_2/propyl-1-(*o*-vanillinaldimine)][$CoCl_2$].

δ_{ppm} 14.4, 19.0, 54.2, 59.7, 96.7, 109.6, 117.3, 120.8, 122.4, 128.2, 129.9, 130.1, 130.9, 132.1, 139.1, 142.5, 145.6, 147.7, 165.4.

2.3.2 Compound (4). Yellow solid; IR (KBr), ν: 728, 845, 1088, 1246, 1457, 1515, 1573, 1618, 1656, 1698, 2856, 2973, 3236, 3429 cm^{-1}; ^1H NMR (250 MHz, DMSO-d_6), δ_{ppm}: 1.08 (s, 3H, CH_3), 2.06 (s, 3H, CH_3), 3.98 (d, 2H, J = 6.50 Hz, aliphatic), 6.71 (s, 1H, CH), 6.95–7.04 (m, 2H), 7.13 (d, 1H, J = 7.50 Hz, ArH), 7.36–7.54 (m, 4H), 10.97 (s, 1H, NH); ^{13}C NMR (62.5 MHz, DMSO-d_6), δ_{ppm}: 14.5, 19.1, 53.8, 59.8, 109.6, 117.4, 120.9, 22.5, 128.5, 129.3, 132.4, 133.6, 142.5, 145.5, 148.

2.3.3 Compound (6). Yellow solid; IR (KBr), ν: 425, 507, 750, 823, 1010, 1160, 1245, 1458, 1571, 1696, 1731, 1908, 2980, 3382; ^1H NMR (250 MHz, DMSO-d_6), δ_{ppm}: 1.12 (s, 3H, CH_3), 2.44 (s, 2H, CH_2), 3.99 (s, 2H, CH_2), 6.40 (s, 1H, CH), 6.99 (s, 2H, Ar–H), 7.30 (s, 4H, Ar–H), 7.41 (s, 2H, Ar–H), 10.85 (s, 1H, NH); ^{13}C NMR (62.5 MHz, DMSO-d_6), δ_{ppm}: 14.5, 19.0, 55.7, 59.8, 97.8, 110.2, 117.3, 120.7, 121.3, 122.3, 129.7, 131.7, 141.8, 142.7, 145.8, 147.2, 165.5.

2.3.4 Compound (9). White solid; IR (KBr), ν : 501, 763, 872, 1087, 1253, 1340, 1520, 1570, 1600, 1707, 2837, 2928, 2974, 3098, 3432 cm^{-1}; ^1H NMR (250 MHz, DMSO-d_6), δ_{ppm}: 1.12 (s, 3H, CH_3), 2.45 (s, 2H, CH_3), 3.98 (s, 2H, CH_2), 6.57 (s, 1H, CH), 6.98 (m, 2H, ArH), 7.28 (m, 2H, ArH), 7.62 (s, 2H, ArH), 8.10 (s, 2H, ArH), 10.95 (s, 1H, NH); ^{13}C NMR (62.5 MHz, DMSO-d_6), δ_{ppm}: 14.5, 19.2, 55.7, 59.9, 97.2, 110.2, 117.4, 120.9, 122.50, 124.1, 128.9, 131.8, 142.7, 145.7, 147.4, 147.9, 149.4, 165.4.

2.3.5 Compound (11). Yellow solid; IR (KBr), ν: 417, 742, 1079, 1526, 1576, 1618, 1664, 1702, 2930, 3242, 3444 cm^{-1}; ^1H NMR (250 MHz, DMSO-d_6), δ_{ppm}: 1.26 (s, CH_3), 2.48 (s, 3H, CH_3), 3.93 (s, 2H, CH_2), 6.56 (s, 1H, CH), 7.09, (s, 2H, ArH), 7.25 (d, J = 5.00 Hz, 1H, ArH), 7.40, (s, 3H, ArH), 7.55, (s, 1H, ArH), 7.89 (d, J = 7.50, Hz, 1H, ArH), 11.04 (s, 1H, NH); ^{13}C NMR (62.5 MHz, DMSO-d_6), δ_{ppm}: 14.4, 19.4, 51.0, 60.0, 97.8, 110.0, 117.5, 121.2, 122.6, 124.4, 129.6, 132.0, 134.6, 137.2, 145.8, 147.7, 148.2, 165.3.

2.3.6 Compound (13). White solid; IR (KBr), ν: 488, 742, 859, 1030, 1088, 1250, 1460, 1521, 1575, 1661, 1698, 2838, 2979, 3236; ^1H NMR (250 MHz, DMSO-d_6), δ_{ppm}: 1.05 (t, J = 7.50 Hz, 3H, CH_3), 2.48 (s, 3H, CH_3), 3.79 (s, 3H, O–CH_3), 3.94 (t, J = 7.50 Hz, 2H, CH_2), 6.64 (s, 1H, CH), 6.80–6.99 (m, 4H, ArH), 7.15 (d, J = 5.00 Hz, 2H, ArH), 7.28 (d, J = 7.50 Hz, 2H, ArH), 10.69 (s, 1H, NH); ^{13}C NMR (62.5 MHz, DMSO-d_6), δ_{ppm}: 14.3, 18.9, 51.4,

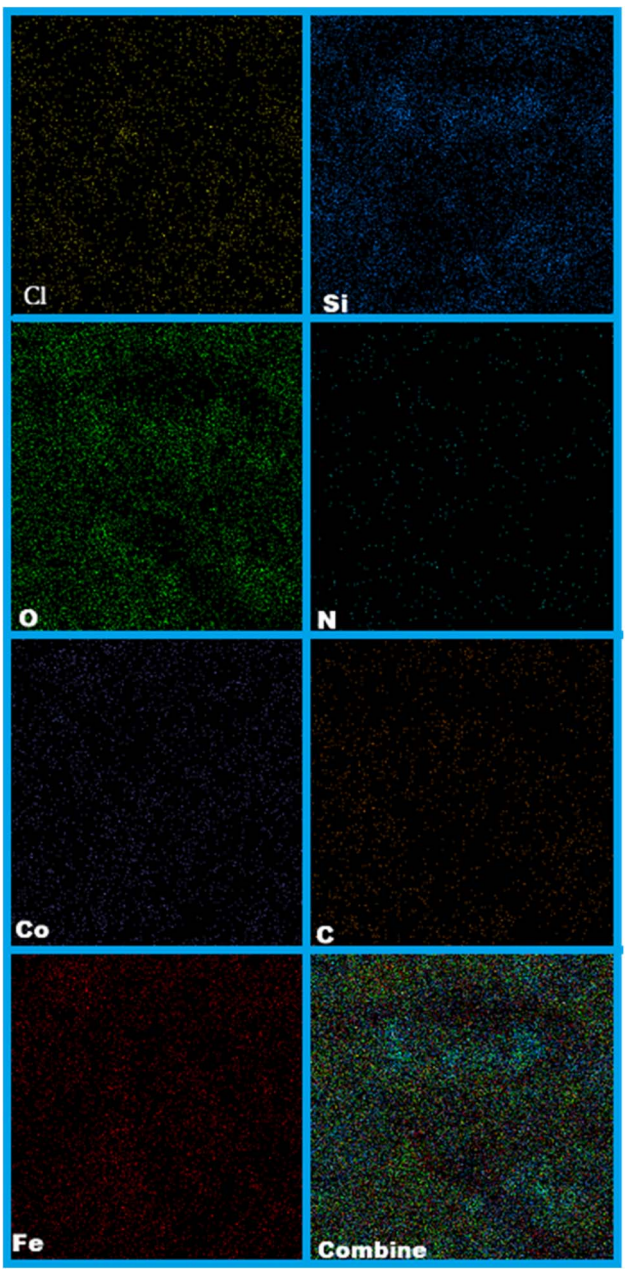

Fig. 3 SEM coupled with EDX (SEM mapping) of nano-[$CoFe_2O_4$@-SiO_2/propyl-1-(*o*-vanillinaldimine)][$CoCl_2$].

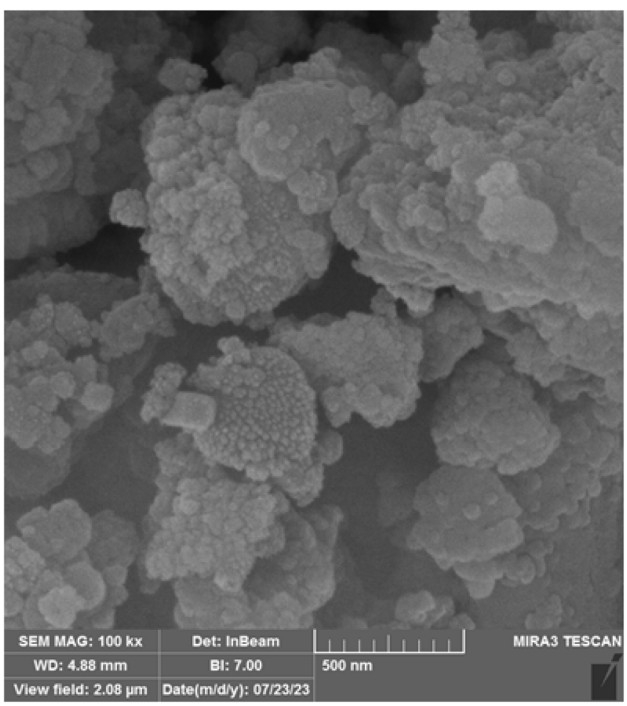

Fig. 4 FESEM analysis of nano-[$CoFe_2O_4$@SiO_2/propyl-1-(*o*-vanillinaldimine)][$CoCl_2$].

55.9, 59.5, 97.0, 109.6, 111.7, 117.0, 120.4, 120.8, 121.9, 129.6, 146.3, 147.4, 146.7.

2.3.7 Compound (14). White solid; IR (KBr), ν: 743, 819, 1048, 1258, 1574, 1619, 1660, 1701, 2835, 2930, 3103 cm^{-1}; ^1H NMR (250 MHz, DMSO-d_6), δ_{ppm}: 0.85 (s, 1H, CH_3), 1.06 (t, 1H, J = 7.5 Hz, CH_3), 2.42 (s, 1H, CH_2), 2.48 (s, 1H, CH_2), 3.61 (s, 3H, CH_3–O), 3.70 (s, 3H, CH_3–O), 3.94 (q, J = 7.5 Hz, 2H, CH_2), 6.64 (s, 1H, CH), 6.93 (s, 1H, Ar–H), 7.01 (d, J = 7.5 Hz, 1H, Ar–H), 7.30 (s, 1H, Ar–H), 7.55 (s, 1H, Ar–H), 7.72 (s, 1H, Ar–H), 8.03 (s, 1H, Ar–H), 8.25 (s, 1H, Ar–H), 10.93 (s, 1H, NH); ^{13}C NMR (62.5 MHz, DMSO-d_6), δ_{ppm}: 14.4, 19.0, 51.7, 55.6, 56.4, 59.5, 96.8, 109.7, 112.8, 113.5, 116.0, 117.0, 120.4, 122.0, 130.8, 132.2, 142.5, 146.2, 147.4, 151.1, 153.3, 165.

3. Results and discussion

In the present work, to design novel cobalt(II) Schiff base complex and immobilize it on a magnetic surface for use as a recoverable catalyst in organic reactions, a Schiff base ligand was first synthesized by reacting *ortho*-vanillin with 3-aminopropyltriethoxysilane. In the next step, the cobalt(II) Schiff base complex was formed by the metalation of the synthesized Schiff base ligand with cobalt(II) chloride. Finally, the cobalt(II) Schiff base complex was immobilized on $CoFe_2O_4$@SiO_2 nanoparticles to prepare the magnetite cobalt(II) Schiff base complex as a reusable catalyst (Scheme 2).

After the preparation of the supported nanomagnetite cobalt(II) Schiff base complex, FT-IR analysis of nano-[$CoFe_2O_4$@SiO_2/propyl-1-(*o*-vanillinaldimine)][$CoCl_2$] was conducted to identify the key bonds in the structure, in comparison with other components of the catalyst (Fig. 1). The analysis demonstrated that the vibrations at 1095 and 596 cm^{-1} corresponded to the Si–O–Si and Fe–O bonds, respectively. The vibration at 2925 cm^{-1} was associated with C–H bond vibration. Additionally, the peak corresponding to the C=N bond of the Schiff base ligand appeared at approximately 1606 cm^{-1}, indicating interaction with cobalt chloride in the prepared complex. This analysis confirmed the presence of the key and desired bonds in the structure of the final catalyst.

In another study, to identify the elements present in the nanomagnetite Schiff base complex, energy-dispersive X-ray spectroscopy (EDX) analysis of nano-[$CoFe_2O_4$@SiO_2/propyl-1-(*o*-vanillinaldimine)][$CoCl_2$] was performed. The analysis indicated that the expected elements, including cobalt, iron, nitrogen, oxygen, carbon, silicon and chlorine were detected in the designed complex (Fig. 2).

To determine the distribution of elements in the designed catalyst structure, SEM coupled with EDX (SEM mapping) analysis was conducted. The study revealed that the expected elements, namely, cobalt, iron, nitrogen, oxygen, silicon, carbon and chlorine, were appropriately distributed within the catalyst structure (Fig. 3).

To determine the contact surface and particle size of the catalyst, field emission scanning electron microscopy (FESEM) analysis of nano-[$CoFe_2O_4$@SiO_2/propyl-1-(*o*-vanillinaldimine)][$CoCl_2$] was performed. The images obtained showed that the particle size of the designed nanomagnetite cobalt(II) Schiff base complex was less than 100 nm (Fig. 4).

The particle size of the presented nanomagnetite cobalt(II) Schiff base complex was also investigated using transmission electron microscopy (TEM). The TEM images revealed that the particles of the prepared catalyst were smaller than 100 nm (Fig. 5). The creation of nano-sized particles enhanced the

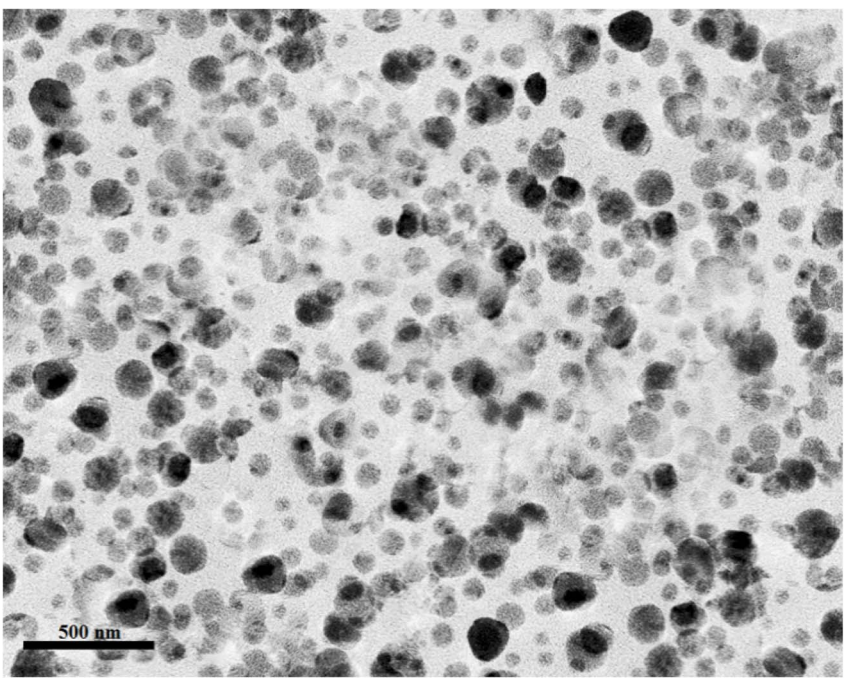

Fig. 5 TEM image of nano-[$CoFe_2O_4$@SiO_2/propyl-1-(*o*-vanillinaldimine)][$CoCl_2$].

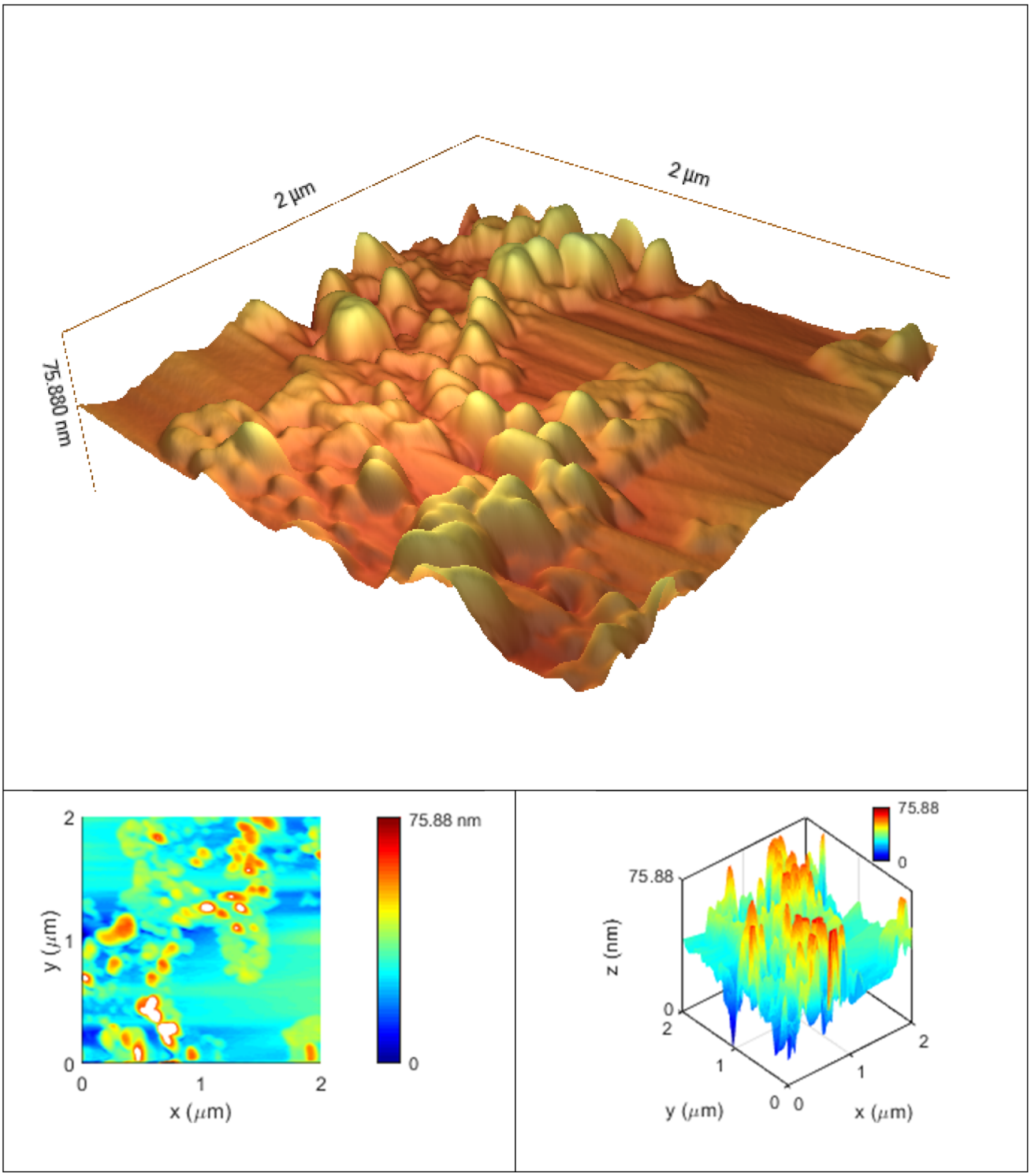

Fig. 6 Atomic force microscopy (AFM) analysis of nano-[$CoFe_2O_4$@SiO_2/propyl-1-(*o*-vanillinaldimine)][$CoCl_2$].

catalytic reaction by increasing the contact surface between the catalyst and the starting materials.

Atomic force microscopy (AFM) analysis is a crucial technique for characterizing nanoparticles, as it provides information on surface topography, nanoparticle size and particle dispersion through atomic force measurements. In this study, the nanoparticles were imaged in both two-dimensional and three-dimensional surface topographies, with a size of 2 microns. Considering the mentioned topographies, a nanoparticle size of 75 nm was observed in the surface topographies, similar to the results from another test conducted. It should be noted that the color changes from blue to red indicated an increase in particle size for the obtained particles (Fig. 6).

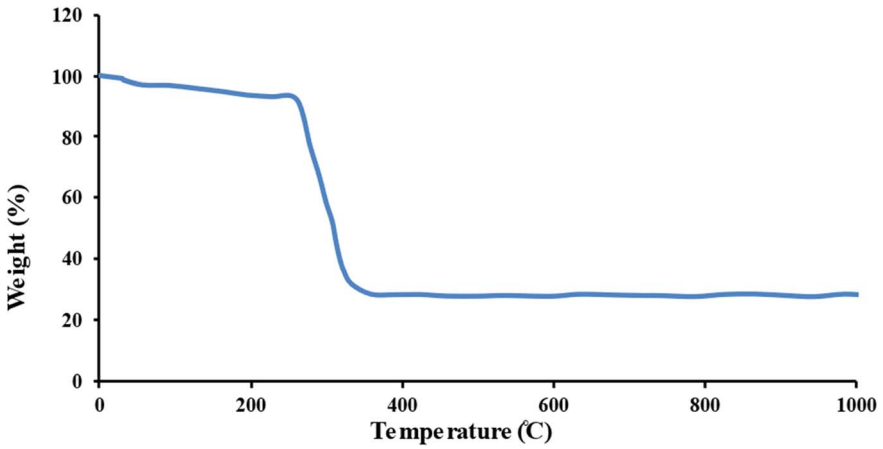

Fig. 7 Thermogravimetric analysis (TGA) of nano-[$CoFe_2O_4$@SiO_2/propyl-1-(*o*-vanillinaldimine)][$CoCl_2$].

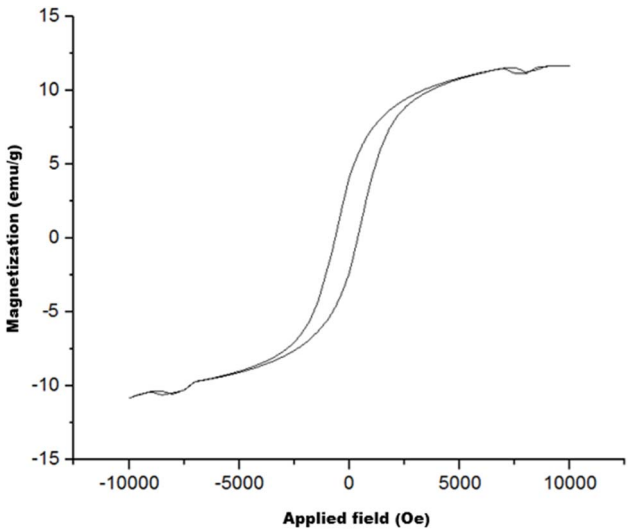

Fig. 8 Vibrating sample magnetometer (VSM) analysis of nano-[$CoFe_2O_4$@SiO_2/propyl-1-(*o*-vanillinaldimine)][$CoCl_2$].

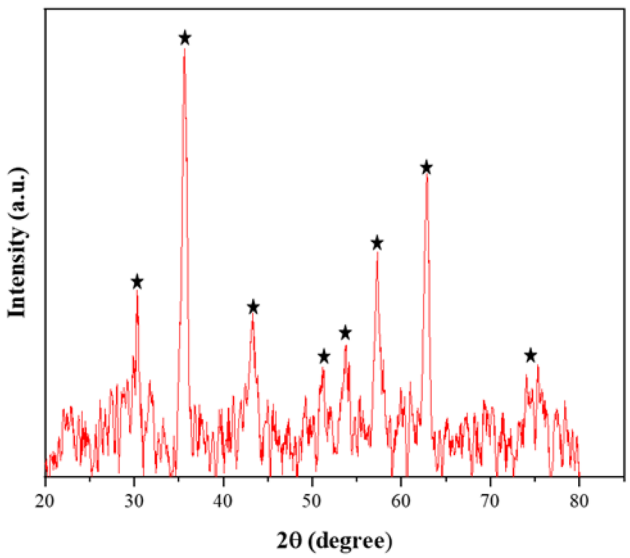

Fig. 9 XRD pattern of nano-[$CoFe_2O_4$@SiO_2/propyl-1-(*o*-vanillinaldimine)][$CoCl_2$].

To assess the thermal stability of the presented magnetite complex and its thermal capacity for use in various reactions, thermogravimetric analysis (TGA) was performed on the nanomagnetite Schiff base complex. The results obtained from this analysis indicated that the prepared catalyst could be used up to a temperature of approximately 300 °C (Fig. 7). As a result, the TGA analysis indicated that this nanomagnetite complex exhibited acceptable thermal tolerance in various organic transformations.

The magnetic activity of [$CoFe_2O_4$@SiO_2/propyl-1-(*o*-vanillinaldimine)][$CoCl_2$] was studied using a vibrating sample magnetometer (VSM) at room temperature to evaluate its separation capability under an external magnetic field. The analysis revealed that the saturation magnetization of [$CoFe_2O_4$@SiO_2/propyl-1-(*o*-vanillinaldimine)][$CoCl_2$] was approximately 12 emu g^{-1}. The saturation magnetization of the prepared nanomagnetite complex is shown in Fig. 8. Based on this analysis, the designed magnetic complex can be effectively used as a recoverable catalyst in various organic transformations.

The X-ray diffraction (XRD) pattern of nano-[$CoFe_2O_4$@SiO_2/propyl-1-(*o*-vanillinaldimine)][$CoCl_2$] was also investigated in the 2θ range of 20–80° (Fig. 9). As shown in Fig. 9, the XRD patterns of the nanomagnetite heterogeneous catalyst exhibited peaks at 2θ ≈ 29.55°, 35.65°, 43.30°, 51.30°, 53.10°, 57.20°, 62.75°, 74.85° and 76.15°.

After the design and characterization of the nanomagnetite cobalt(II) Schiff base complex through various analyses, its catalytic application was studied in the preparation of several 4*H*-pyrimido[2,1-*b*]benzimidazole derivatives. For this purpose, the condensation reaction of 4-nitrobenzaldehyde, 2-aminobenzimidazole and ethyl acetoacetate was selected as a model reaction. Various conditions, including catalyst amount, temperature and solvent types, were tested for the reaction. The

Table 1 Optimization of the reaction conditions for the model reaction

Entry	Solvent	Catalyst amount (mg)	Temp. (°C)	Time (min)	Yield[a] (%)
1	—	—	90	120	27
2	—	1	90	20	38
3	—	2	90	20	54
4	—	3	90	20	95
5	—	6	90	20	95
6	—	3	50	20	30
7	—	3	70	20	72
8	—	3	110	20	90
9	Ethyl acetate	3	Reflux	20	60
10	$CHCl_3$	3	Reflux	20	87
11	EtOH	3	Reflux	20	59
12	CH_2Cl_2	3	Reflux	20	75
13	*n*-Hexane	3	Reflux	20	39
14	DMF	3	Reflux	20	48

[a] Isolated yield.

mentioned reaction was tested in the presence of the designed catalyst, varying from 1 to 6 mg, and at temperatures ranging from 50 to 110 °C. The best results were obtained using 3 mg of catalyst at 90 °C in the absence of solvent. Furthermore, the reaction was studied in different solvents, including ethyl acetate, $CHCl_3$, CH_2Cl_2, *n*-hexane and DMF, and compared with the solvent-free condition. The results were not superior to those obtained under solvent-free conditions (Table 1). Since the catalyst was heterogeneous, the presence of a solvent hindered the contact between the starting materials and the catalyst, leading to a slower reaction and a reduced product yield.

To compare the catalytic activity of the designed nanomagnetite Schiff base complex with its constituent components, the selected reaction was investigated in the presence of each catalyst component individually. The results of this investigation revealed that the catalytic activity of these components was not as effective as that of nano-[$CoFe_2O_4$@SiO_2/propyl-1-(*o*-vanillinaldimine)][$CoCl_2$] (Table 2).

After determining the optimal reaction conditions in the previous study, different aromatic aldehydes, including those with electron-withdrawing groups, electron-donating groups and halogens on their aromatic rings, were used in the reaction with ethyl acetoacetate and 2-aminobenzimidazole to prepare 4*H*-pyrimido[2,1-*b*]benzimidazole derivatives. The corresponding products were obtained with acceptable results (Scheme 3). All reactions were carried out by reacting various aromatic aldehydes with ethyl acetoacetate and 2-aminobenzimidazole in the presence of 3 mg of the nanomagnetite catalyst at 90 °C under solvent-free conditions.

Based on the structure of the prepared complex, the presence of bulky groups on the nitrogen atoms in the cobalt(II) Schiff base ligand structure can lead to a reduction in repulsion. As a result, the cobalt complex may undergo a structural rearrangement, shifting from a tetrahedral form to a square-planar configuration. Based on the calculations, the energy difference between these two structures is not significant, with the tetrahedral arrangement being only 18 kcal more stable than the square-planar arrangement. Therefore, these two structures can exist in equilibrium with each other. The complex adopting a square-planar arrangement could serve as a precursor for the cobalt to achieve a coordination number of six, enabling it to interact with the starting materials and catalyze the reaction (Scheme 4).

3.1. Computational methods

Calculations were performed using the Gaussian 09 system[50] with the B3LYP/6-31G(d) method and basis set.[51,52] Frequency calculations were performed at the same computational level to

Table 2 Catalytic activity of various components of the catalyst in comparison with the main catalyst for the model reaction. All reactions were carried out using 3 mg of the catalyst at 90 °C under solvent-free conditions

Entry	Catalyst	Catalyst amount (mg)	Temp. (°C)	Time (min)	Yield[a] (%)
1	$CoCl_2 \cdot 6H_2O$	3	90	20	32
2	$CoFe_2O_4$@SiO_2	3	90	20	60
3	Schiff base ligand	3	90	20	75
4	Schiff base complex	3	90	20	87
5	Main catalyst	3	90	20	95

[a] Isolated yield.

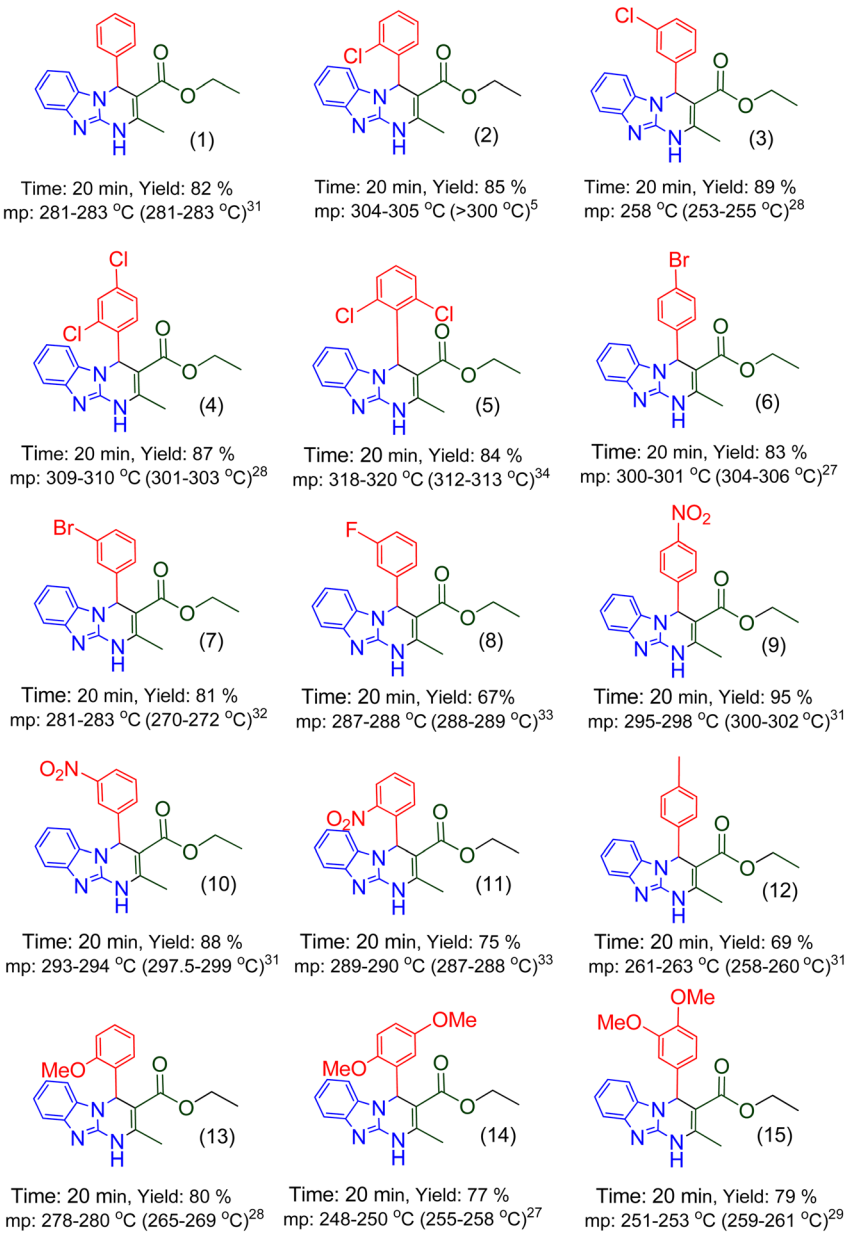

Scheme 3 Synthesis of 4*H*-pyrimido[2,1-*b*]benzimidazoles. All reactions were carried out using 3 mg of nanomagnetite catalyst at 90 °C under solvent-free conditions.

confirm that the obtained structures corresponded to energy minima.

The internal energies of the tetrahedral and square-planar structures were −3917.848479 and −3917.819183 hartree, respectively. Based on the calculated internal energies in the gas phase, the tetrahedral geometry was slightly more stable (by about −18 kcal mol^{-1}) than the square-planar structure. It appeared that the two geometries were in equilibrium, with a slight preference for the tetrahedral geometry (Fig. 10).

In the proposed mechanism, the cobalt complex in its tetrahedral form rearranged to a square-planar structure, and aldehyde and ethyl acetoacetate in their enol form were added to this complex, allowing cobalt to achieve six coordination. According to the calculations, the transition from tetrahedral to square-planar arrangement required minimum energy. In the next step of the reaction, the nucleophilic attack of ethyl acetoacetate in its enol form occurred on the activated aldehyde, forming intermediate (**I**). Additionally, the chloride anion generated from the cobalt complex served as a base, reacting with the acidic hydrogen in the structure of ethyl acetoacetate to facilitate the Knoevenagel reaction. Subsequently, 2-aminobenzimidazole could replace the aldehyde in the empty coordination site of the cobalt complex and react with intermediate (**I**) as a Michael acceptor, forming intermediate (**II**), which then underwent tautomerization to yield the keto form (**III**). Through the intramolecular nucleophilic attack of the imine group on the carbonyl group of intermediate (**III**), which was activated by the cobalt complex, intermediate (**IV**) was formed. Finally, by the removal of

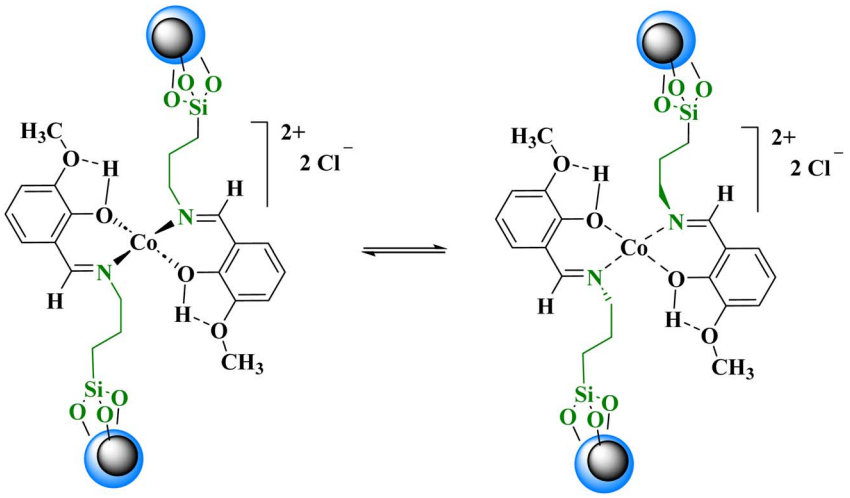

Scheme 4 Conversion from tetrahedral to square-planer arrangement for the cobalt complex.

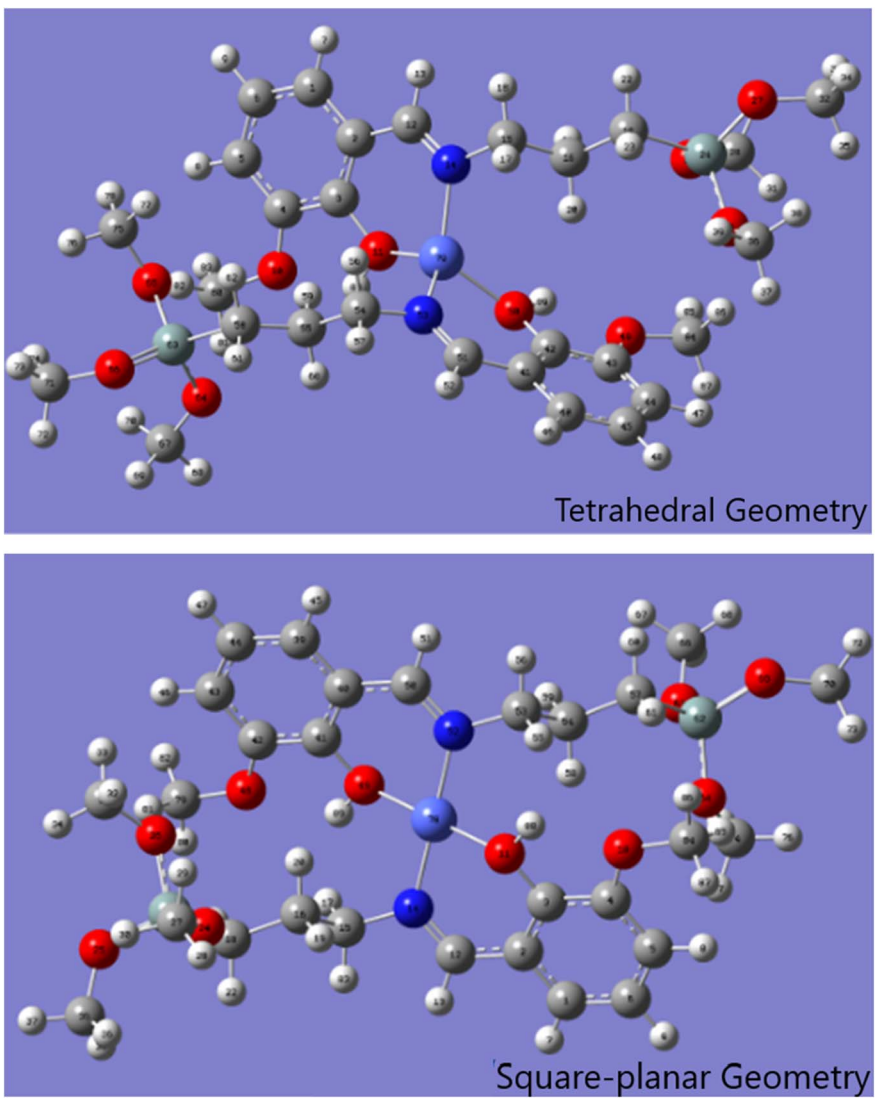

Fig. 10 Structure of the nanomagnetite cobalt complex in tetrahedral and square-planar forms.

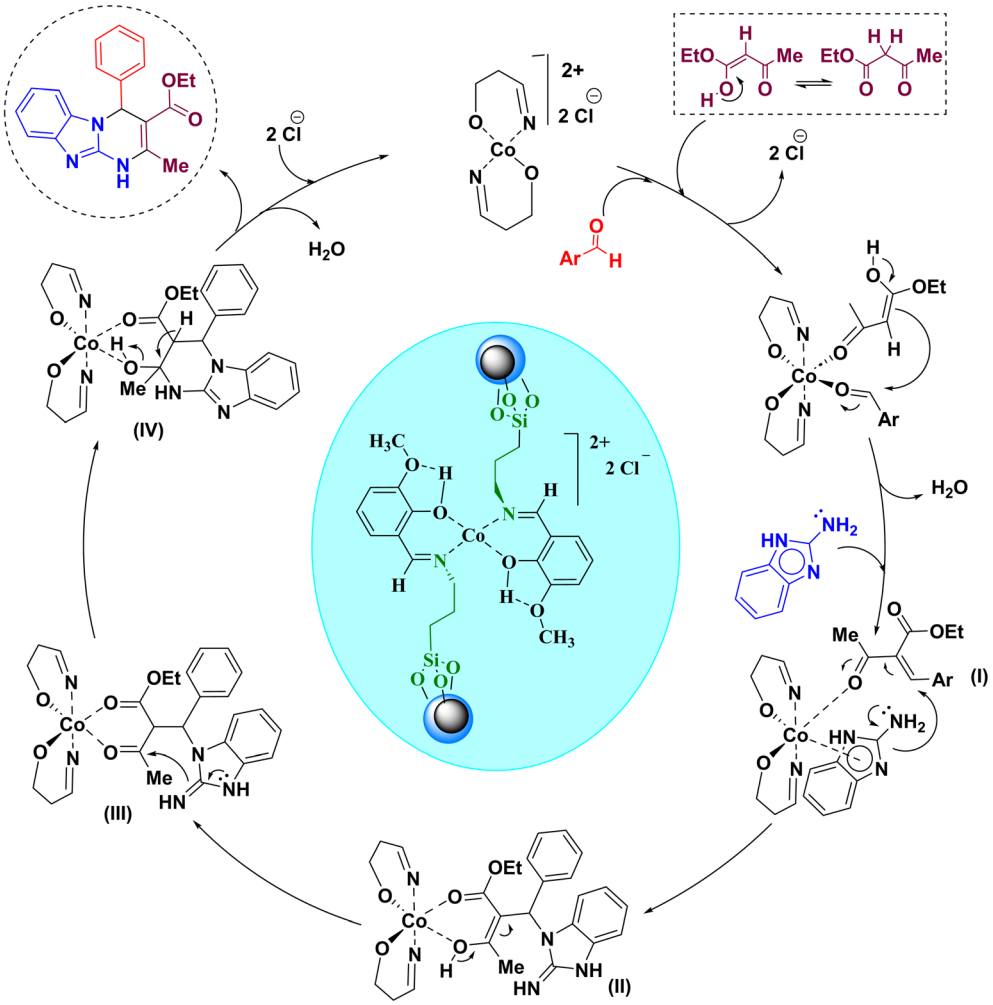

Scheme 5 Proposed mechanism for the synthesis of 4*H*-pyrimido[2,1-*b*]benzimidazoles.

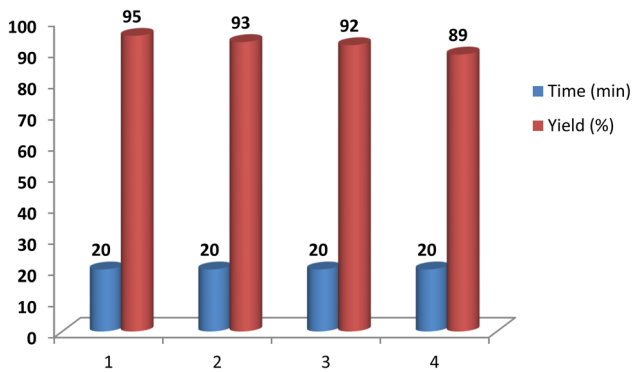

Fig. 11 Recovery of nano-[$CoFe_2O_4$@SiO_2/propyl-1-(*o*-vanillinaldimine)][$CoCl_2$].

one molecule of H_2O, a process activated by the cobalt complex and accelerated by the chloride anion generated from the cobalt complex, the main product was obtained (Scheme 5). According to the proposed mechanism, the rearrangement of the cobalt complex from a tetrahedral to a square-planar form increased the coordination number of cobalt. This rearrangement activated the cobalt complex, allowing the starting materials to bind as ligands and position themselves in close proximity, facilitating their reaction in the correct orientation.

Placing the Schiff base cobalt(II) complex on the nano-magnetite substrate allowed for the easy separation of the catalyst from the reaction mixture. To assess this, the recovery of the catalyst was investigated in the reaction of 4-nitrobenzaldehyde, 2-aminobenzimidazole and ethyl acetoacetate. At the end of the reaction, the mixture was extracted with warm ethanol, and the catalyst was separated from the reaction mixture using an external magnet. The isolated catalyst was recovered and used in subsequent reactions after being washed with acetone. Catalyst recovery was performed three times without a notable decrease in reaction yield or any change in reaction time. The results of this study are presented in Fig. 11. The recovery and reuse of the catalyst not only save raw materials but also help prevent environmental pollution, which is one of the important advantages of using the designed catalyst.

To demonstrate the accuracy, the structure of the reused catalyst was investigated by FT-IR analysis and compared with that of the fresh catalyst (Fig. 12). According to Fig. 12, the FT-IR

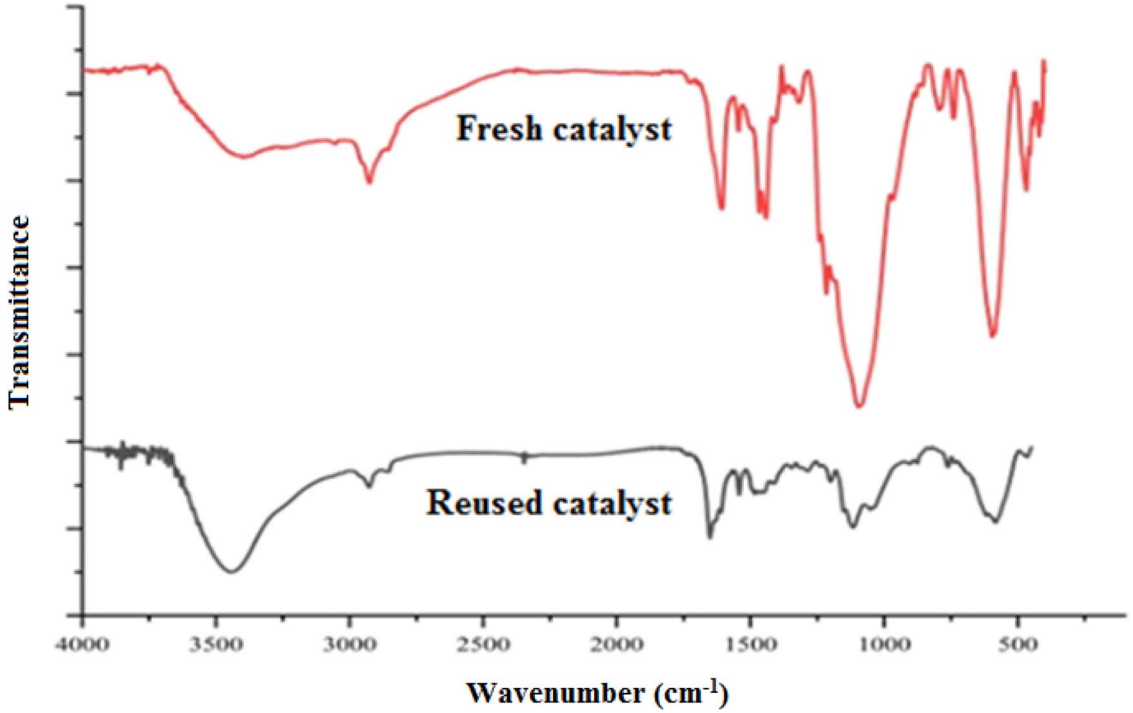

Fig. 12 FT-IR spectra of the reused catalyst in comparison with the fresh catalyst.

Table 3 Comparison of bond vibrations in the reused and fresh catalysts

Reused catalyst		Fresh catalyst	
Bond	Wavenumber (cm^{-1})	Bond	Wavenumber (cm^{-1})
Co–O	450	Co–O	468
Fe–O	595	Fe–O	596
Si–O–Si	1095	Si–O–Si	1095
C=N	1703	C=N	1606
C–H	2928	C–H	2925
O–H	3409	O–H	3373

spectrum of the reused catalyst matched that of the fresh catalyst. The bond vibrations for various bonds in the reused catalyst were compared with those in the fresh catalyst and are presented in Table 3.

To investigate the reason for the decrease in product yield with the reused catalyst, the leaching of cobalt from the surface of the catalyst was investigated using atomic absorption spectroscopy. The investigation revealed that the fresh catalyst contained 12.89% cobalt, while the recovered catalyst, after being used four times, contained 11.01% cobalt. As a result, leaching of cobalt from the magnetically supported cobalt(II) Schiff base complex can lead to a reduction in the product yield.

4. Conclusions

In summary, we have synthesized and fully characterized nano-[$CoFe_2O_4$@SiO_2/propyl-1-(*o*-vanillinaldimine)][$CoCl_2$] through various analyses, introducing it as a magnetically supported Schiff base cobalt(II) complex. This complex served as an effective catalyst for the three-component preparation of 4*H*-pyrimido[2,1-*b*]benzimidazoles, *via* the reaction of 2-aminobenzimidazole with ethyl acetoacetate and various aromatic aldehydes, yielding high product yields and suitable reaction times at 90 °C under solvent-free conditions.

Data availability

The datasets supporting this article have been uploaded as part of the ESI.†

Conflicts of interest

There are no conflicts to declare.

References

1 M. T. Gabr, N. S. El-Gohary, E. R. El-Bendary and M. M. El-Kerdawy, *Eur. J. Med. Chem.*, 2014, **85**, 576–592.
2 S. Nalawade, V. Deshmukh and S. Chaudhari, *J. Pharma Res.*, 2013, **7**, 433–438.
3 H. Sheibani and M. Babaie, *Russ. Chem. Bull.*, 2013, **62**, 2202–2208.
4 P. H. Tran, T.-P. T. Bui, X.-Q. B and Lam and X.-T. T. Nguyen, *RSC Adv.*, 2018, **8**, 36392–36399.
5 R. Talaei and A. Olyaei, *Iran. J. Catal.*, 2016, **6**, 339–343.
6 M. Farajpour, S. M. Vahdat, S. M. Baghbanian and M. Hatami, *Chem. Methodol.*, 2023, **7**, 540–551.

7 R. M. Muhiebes, L. Fatolahi and S. Sajjadifar, *Asian J. Green Chem.*, 2023, **7**, 121–131.
8 Y. Ghalandarzehi and H. Kord-Tamandani, *Asian J. Green Chem.*, 2023, **7**, 70–84.
9 M. A. Amiri, H. Younesi, H. K. Aqmashhadi, G. F. Pasha, S. Asghari and M. Tajbakhsh, *Chem. Methodol.*, 2024, **8**, 1–22.
10 R. M. Mhaibes, Z. Arzehgar, M. M. Heydari and L. Fatolahi, *Asian J. Green Chem.*, 2023, **7**, 1–8.
11 H. Ghafuri, M. Zargari and A. Emami, *Asian J. Green Chem.*, 2023, **7**, 54–69.
12 M. kidwai, P. Dwivedi and A. Jahan, *J. Appl. Organomet. Chem.*, 2023, **3**, 156–168.
13 B. Baghernejad and M. Fiuzat, *J. Med. Nanomater. Chem.*, 2023, **5**, 235–242.
14 A. R. Moosavi-Zare, M. A. Zolfigol, E. Noroozizadeh, O. Khaledian and B. S. Shaghasemi, *Res. Chem. Intermed.*, 2016, **42**, 4759–4772.
15 A. R. Moosavi-Zare, M. A. Zolfigol, E. Noroozizadeh, M. Zarei, R. Karamian and M. Asadbegy, *J. Mol. Catal. A:Chem.*, 2016, **425**, 217–228.
16 M. A. Zolfigol, S. Baghery, A. R. Moosavi-Zare and S. M. Vahdat, *J. Mol. Catal. A: Chem.*, 2015, **409**, 216–226.
17 A. R. Moosavi-Zare, M. A. Zolfigol and A. Mousavi-Tashar, *Res. Chem. Intermed.*, 2016, **42**, 7305–7312.
18 H. R. Shaterian, N. Fahimi and K. Azizi, *Res. Chem. Intermed.*, 2014, **40**, 1879–1898.
19 A. Shaabani, A. Rahmati and S. Naderi, *Bioorg. Med. Chem. Lett.*, 2005, **15**, 5553–5557.
20 S. Azad and B. F. Mirjalili, *Res. Chem. Intermed.*, 2017, **43**, 1723–1734.
21 N. Shekarlab, R. Ghorbani-Vaghei and S. Alavinia, *Appl. Organomet. Chem.*, 2020, e5918.
22 P. K. Sahu, P. K. Sahu, Y. Sharma, D. D. Agarwal and J. Heterocyclic, *Chem*, 2014, **51**, 1193–1198.
23 C. Yao, S. Lei, C. Wang, T. Li, C. Yu, X. Wang and S. Tu, *J. Heterocycl. Chem.*, 2010, **47**, 26–32.
24 N. Basirat, S. S. Sajadikhah and A. Zare, *Res. Chem. Intermed.*, 2020, **46**, 3263–3275.
25 M. Abedini, F. Shirini, M. Mousapour and O. Goli-Jolodar, *Res. Chem. Intermed.*, 2016, **42**, 6221–6229.
26 J. Liu, M. Lei and L. Hu, *Green Chem.*, 2012, **14**, 840–846.
27 Z. Jalilian, A. R. Moosavi-Zare, M. Ghadermazi and H. Goudarziafshar, *RSC Adv.*, 2023, **13**, 10642–10649.
28 R. Ghorbani-Vaghei, Z. Toghraei-Semiromi, R. Karimi-Nami and Z. Salimi, *Helv. Chim. Acta*, 2014, **97**, 979–984.
29 A. R. Moosavi-Zare, H. Goudarziafshar and P. Fashi, *Res. Chem. Intermed.*, 2020, **46**, 5567–5582.
30 H. Goudarziafshar, N. Taheriazod and A. R. Moosavi-Zare, *Appl. Catal. O: Open*, 2024, **193**, 206970.
31 M. Makhsous, F. Shirini, M. Seddighi and M. Mazloumi, *Polycyclic Aromat. Compd.*, 2020, **40**, 494–501.
32 M. Mashhadinezhad, F. Shirini, M. Mamaghani and M. Rassa, *Polycyclic Aromat. Compd.*, 2020, **40**, 1417–1433.
33 A. Thongni, R. Nongkhlaw, C. Pandya, A. Sivaramakrishna, P. M. Gannon and W. Kaminsky, *J. Heterocycl. Chem.*, 2024, **61**, 581–599.
34 R. Alajarin, J. J. Vaquero, J. Alvarez-Builla, M. F. d. Casa-Juana, C. Sunkel, J. G. Priego, P. Gomez-Salcpd and R. Torres, *Bioorg. Med. Chem.*, 1994, **2**, 323–329.
35 A. R. Moosavi-Zare, M. A. Zolfigol, V. Khakyzadeh, C. Böttcher, M. H. Beyzavi, A. Zare, A. Hasaninejad and R. Luque, *J. Mater. Chem. A*, 2014, **2**, 770–777.
36 A. R. Moosavi-Zare, M. A. Zolfigol, F. Derakhshan-Panah and S. Balalaie, *Mol. Catal.*, 2018, **449**, 142–151.
37 L. V. Chopda and P. N. Dave, *Results Chem.*, 2021, **3**, 100169.
38 L. V. Chopda and P. N. Dave, *Arabian J. Chem.*, 2020, **13**, 5911–5921.
39 L. V. Chopda and P. N. Dave, *Chemistryselect*, 2020, **5**, 5552–5572.
40 L. V. Chopda and P. N. Dave, *Chemistryselect*, 2020, 2395–2400.
41 A. R. Moosavi-Zare, R. Najafi and H. Goudarziafshar, *RSC Adv.*, 2024, **27**, 19167–19173.
42 A. Gorji, S. Esmaili, A. R. Moosavi-Zare and A. Khazaei, *J. Mol. Struct.*, 2024, **1314**, 138797.
43 H. Goudarziafshar, M. Zafari and A. R. Moosavi-Zare, *RSC Adv.*, 2024, **14**, 27565–27574.
44 H. Goudarziafshar, M. Zafari and A. R. Moosavi-Zare, *Chem. Methodol.*, 2024, **8**, 820–832.
45 Z. Jalilian, A. R. Moosavi-Zare and M. Ghadermazi, *Chem. Methodol.*, 2025, **9**, 326–342.
46 A. R. Moosavi-Zare, H. Goudarziafshar and Z. Jalilian, *Appl. Organomet. Chem.*, 2019, **33**, e4584.
47 A. R. Moosavi-Zare, H. Goudarziafshar and Z. Bahrami, *Res. Chem. Intermed.*, 2023, **49**, 507–523.
48 A. R. Moosavi-Zare, H. Goudarziafshar and K. Saki, *Appl. Organomet. Chem.*, 2018, **32**, e3968.
49 M. Aliavazi, M. H. Ardakani and A. Naeimi, *Inorg. Chem. Commun.*, 2024, **160**, 111895.
50 M. J. Frisch, G. W. Trucks, H. B. Schlegel, G. E. Scuseria, M. A. Robb, J. R. Cheeseman, G. Scalmani, V. Barone, B. Mennucci, G. A. Petersson, H. Nakatsuji, M. Caricato, X. Li, H. P. Hratchian, A. F. Izmaylov, J. Bloino, G. Zheng, J. L. Sonnenberg, M. Hada, M. Ehara, K. Toyota, R. Fukuda, J. Hasegawa, M. Ishida, T. Nakajima, Y. Honda, O. Kitao, H. Nakai, T. Vreven, J. A. Montgomery Jr, J. E. Peralta, F. Ogliaro, M. Bearpark, J. J. Heyd, E. Brothers, K. N. Kudin, V. N. Staroverov, T. Keith, R. Kobayashi, J. Normand, K. Raghavachari, A. Rendell, J. C. Burant, S. S. Iyengar, J. Tomasi, M. Cossi, N. Rega, J. M. Millam, M. Klene, J. E. Knox, J. B. Cross, V. Bakken, C. Adamo, J. Jaramillo, R. Gomperts, R. E. Stratmann, O. Yazyev, A. J. Austin, R. Cammi, C. Pomelli, J. W. Ochterski, R. L. Martin, K. Morokuma, V. G. Zakrzewski, G. A. Voth, P. Salvador, J. J. Dannenberg, S. Dapprich, A. D. Daniels, O. Farkas, J. B. Foresman, J. V. Ortiz, J. Cioslowski, and D. J. Fox ,*Gaussian 09, Revision B.01*, Gaussian Inc., Wallingford, 2010.
51 P. J. Hay and W. R. Wad, *J. Chem. Phys.*, 1985, **82**, 299–310.
52 A. E. Reed, R. B. Weinstock and F. Winhold, Natural population analysis, *J. Chem. Phys.*, 1985, **83**, 735–746.